DINAME 2017 - Proceedings of the XVII International Symposium on Dynamic Problems of Mechanics
A. T. Fleury, D. A. Rade, P. R. G. Kurka (Editors), ABCM, São Sebastião, SP, Brazil, March 5-10, 2017

Flexural Wave Band Gaps in a 1D Phononic Crystal Beam

Edson Jansen Pedrosa de Miranda Júnior[1,2], **José Maria Campos dos Santos**[1]

[1] Department of Computational Mechanics, Faculty of Mechanical Engineering, University of Campinas, Mendeleyev Street, 200, Cidade Universitária "Zeferino Vaz", Barão Geraldo, 13083860, Campinas, SP, Brazil, edson.jansen@ifma.edu.br, zema@fem.unicamp.br

[2] Department of Professional Education, Itaqui-Bacanga Centre, Centro Histórico Campus, Federal Institute of Education, Science and Technology of Maranhão, Afonso Pena Street, 174, Centro, 65010030, São Luís, MA, Brazil

Abstract: In this study, it is investigated theoretically and experimentally the forced response of elastic waves propagating in a 1D phononic crystal (PC) beam and its band structure. The PC beam unit cell is composed by steel and polyethylene. The study is performed by using six methods, the finite element (FE), spectral element (SE), wave finite element (WFE), wave spectral element (WSE), conventional plane wave expansion (CPWE) and improved plane wave expansion (IPWE). Simulated examples of 1D PC beam, considering unit cells of different sizes, with Bragg-type gaps, are calculated. The forced response results are presented in the form of displacement, transmittance and receptance, and the elastic band structure is investigated using its real and imaginary (attenuation) parts. The numerical results of all methods are in a good agreement, except by the limitation of WFE and FE methods in high frequencies. It is also studied the polyethylene quantity influence on the attenuation constant. Depending on the application, choosing the polyethylene quantity correctly is not simple, because it is related to the unit cell size and in which frequency the band gap start. An experiment of a 1D PC beam is proposed and the numerical results can localize the band gap position and width close to the experimental results. A small Bragg-type gap with low attenuation is observed between 405 Hz – 720 Hz. The 1D PC beam with unit cells of steel and polyethylene presents potential application for vibration control.

Keywords: 1D phononic crystal beam, flexural vibration, band gaps, vibration control.

INTRODUCTION

Artificial periodic composites known as phononic crystals (PCs), consisting of a periodic array of scatterers embedded in a host medium, have been quite studied (SIGALAS and ECONOMOU, 1994; KUSHWAHA *et al.*, 1994; PENNEC *et al.*, 2010; HUANG and SHI, 2013; YU *et al.* 2013; ANJOS and ARANTES, 2015; MIRANDA JÚNIOR and DOS SANTOS, 2015; MIRANDA JÚNIOR and DOS SANTOS, 2016a; MIRANDA JÚNIOR and DOS SANTOS, 2016b). PCs have received renewed attention because they exhibit complete band gaps where mechanical (elastic or acoustic) wave propagation is forbidden. The physical origin of phononic and photonic band gaps can be understood at micro-scale using the classical wave theory to describe the Bragg and Mie resonances, respectively, based on the scattering of mechanical and electromagnetic waves propagating within the crystal (OLSSON III and EL-KADY I, 2009).

PCs can be applied in many situations, such as vibration isolation technology (JENSEN, 2003; WANG *et al.* 2005; CASADEI *et al.*, 2012; MIRANDA JÚNIOR and DOS SANTOS, 2016c; MIRANDA JÚNIOR and DOS SANTOS, 2016d), acoustic barriers/filters (HO *et al.*, 2003; QIU *et al.*, 2005; YANG *et al.*, 2010), noise suppression devices (CASADEI *et al.* 2010; XIAO *et al.* 2012) and surface acoustic devices (BENCHABANE *et al.*, 2006).

Most of the studies concerning PCs focused on investigation of bulk mechanical waves (SIGALAS and ECONOMOU, 1994; KUSHWAHA *et al.*, 1994; PENNEC *et al.*, 2010; HUANG and SHI, 2013; YU *et al.*, 2013; ANJOS and ARANTES, 2015; MIRANDA JÚNIOR and DOS SANTOS, 2016a) and its results have shown that the band gaps may appear because of the contrast between the physical properties, for instance elastic modulus and density of the inclusions and matrix. Other important properties that influence the band gap width are the inclusion geometry, inclusion shape, filling fraction and PC lattice. The band gaps may also be affected by the physical nature of PC, which can be: solid/solid (YU *et al.*, 2013; ANJOS and ARANTES, 2015; MIRANDA JÚNIOR and DOS SANTOS, 2016a), fluid/fluid (KUSHWAHA and HALEVI, 1996) and mixed solid/fluid PCs (KUSHWAHA, 1997).

Only few studies have focused on 1D PC (WEN *et al.*, 2005; JIAN-YU *et al.*, 2009; WU *et al.*, 2009; NI *et al.*, 2012, ZHANG *et al.*, 2012; ZHANG *et al.*, 2013; NI *et al.*, 2014; MIRANDA JÚNIOR and DOS SANTOS, 2015) and all of them considered solid/solid PC. However, only Miranda Júnior and Dos Santos (2015) began to study the influence of the polymer quantity variation, inside the PC beam unit cell, on the attenuation constant.

In this context, the main purpose of this study is to investigate the Bragg band gap formation, band structure, also

known as dispersion relation, and attenuation constant of a 1D PC beam using the finite element (FE), spectral element (SE), wave finite element (WFE), wave spectral element (WSE), conventional plane wave expansion method (CPWE) and improved plane wave expansion (IPWE) methods.

THE MODEL AND METHOD

Figure 1 sketches a PC beam with a periodic array of unit cells containing two different materials, *i.e.* steel (blue) and polyethylene (white).

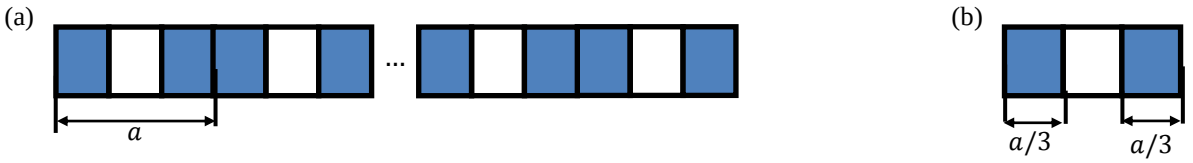

Figure 1 – (a) Schematic representation of PC beam with *N* unit cells of steel (blue) and polyethylene (white). (b) PC beam unit cell.

The PC beam lattice parameter is a. Each unit cell is composed by 2/3 of aluminum and 1/3 of polyethylene. It is important to mention that it is used the Euler-Bernoulli (EB) beam theory. It is not show in details the mathematical formulation of the methods described above because of the pages limitation, however, references are cited.

SE and FE methods

The EB beam mathematical formulation using SE and FE methods can be found in Doyle (1997) and Petyt (2010), respectively. The dynamic stiffness matrices using SE and FE methods can also been found in Miranda Júnior and Dos Santos (2016d). Each unit cell is discretized in three spectral elements using the SE method, *i.e.* each part of unit cell, Fig. 1 (b), corresponds to a one spectral element. However, for the FE method, each part of the unit cell is discretized, Fig. 1 (b), in two finite elements. Thus, the global dynamic stiffness matrix can be obtained by the assembly of the dynamic stiffness matrices of the EB beam elements modeled by SE and FE methods.

WSE and WFE methods

The mathematical formulation of WSE and WFE methods is found in Miranda Júnior and Dos Santos (2016d) and Mencik (2010), respectively. The main difference between WSE and WFE method is the dynamic stiffness matrix used, *i.e.* the dynamic stiffness matrix can be derived from the SE and FE methods, respectively. The main advantage of WSE and WFE methods in relation to the SE and FE methods is the possibility of invoking the Floquet-Bloch's theorem (FLOQUET, 1883; BLOCH, 1928).

CPWE and IPWE methods

The CPWE method, also known as $\omega(K)$ method, is an analytical method to predict the band structure. The CPWE method presents a slow convergence, mainly for systems with a large properties mismatch. To solve this convergence problem, it is used the IPWE method. Cao *et al.* (2004) proposed the IPWE method and showed that this method provides much more accurate numerical results than the CPWE. The mathematical formulation of the IPWE can be found in Li (1996) and Cao *et al.* (2004). The IPWE method application for an EB beam can be found in Wen *et al.* (2005) and Ni *et al.* (2012).

RESULTS AND DISCUSSION

Numerical validation

The EB PC beam parameters and material properties are summarized in Table 1, where the subscripts *A* and *B* refer to steel and polyethylene, respectively.

Table 1 – Beam geometric parameters and material properties.

Geometry/Property	Value
Unit cell length $(a = 2a_A + a_B), a_A = a_B = \frac{1}{3}a$	0.0424 m
Beam length (WSE, WFE, FE and SE methods) (L)	0.424 m
Beam length (CPWE and IPWE methods) (L)	∞
Number of unit cells (WSE, WFE, FE and SE methods) (N)	10
Circular cross section area $(S = \pi r^2, r = 9.45\ mm)$	2.8055 x 10^{-4} m^2
Young's modulus (E_A, E_B)	21 x 10^{10} Pa, 0.72 x 10^{9} Pa
Mass density (ρ_A, ρ_B)	7800 kg/m^3, 935 kg/m^3
Loss factor (η_A, η_B)	0.0013, 0.01
Second moment of area $(I = \pi r^4/4)$	6.2635 x 10^{-9} m^4

Note that the hysteretic damping's, η_A, η_B, also known as loss factors, are included as a complex Young's modulus, $E_A = E_A(1 + i\eta_A)$, $E_B = E_B(1 + i\eta_B)$.

The forced response of the PC beam is analyzed considering a free-free boundary condition and an excitation force as a cosine-shaped pulse only on the left side of the beam. Figure 2 shows the PC beam displacement of left (first node) and right (last node) sides.

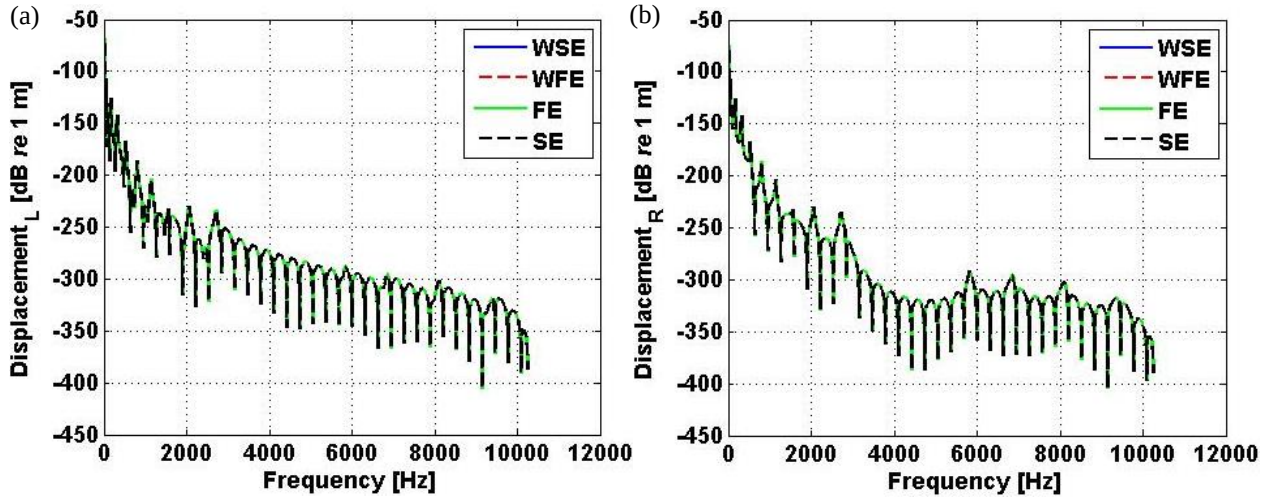

Figure 2 – PC beam displacement of the left (a) side, first node, and right (b) side, last node, calculated by WSE, WFE, FE and SE methods.

As can be seen in Fig. 2 some regions where the resonances do not appear, however, it is difficult to localize exactly the band gaps. To overcome this limitation, it is plotted in Fig. 4 the transmittance, defined as the division between the displacements of the last and first nodes, and the frequency response function (FRF) in Fig. 3(a-b). For the FRF, it is chosen the receptance, *i.e.* the division between the displacement of the first or the last nodes, and the force, which gives H_{11} or H_{12}, respectively, also known as point receptance and transfer receptance.

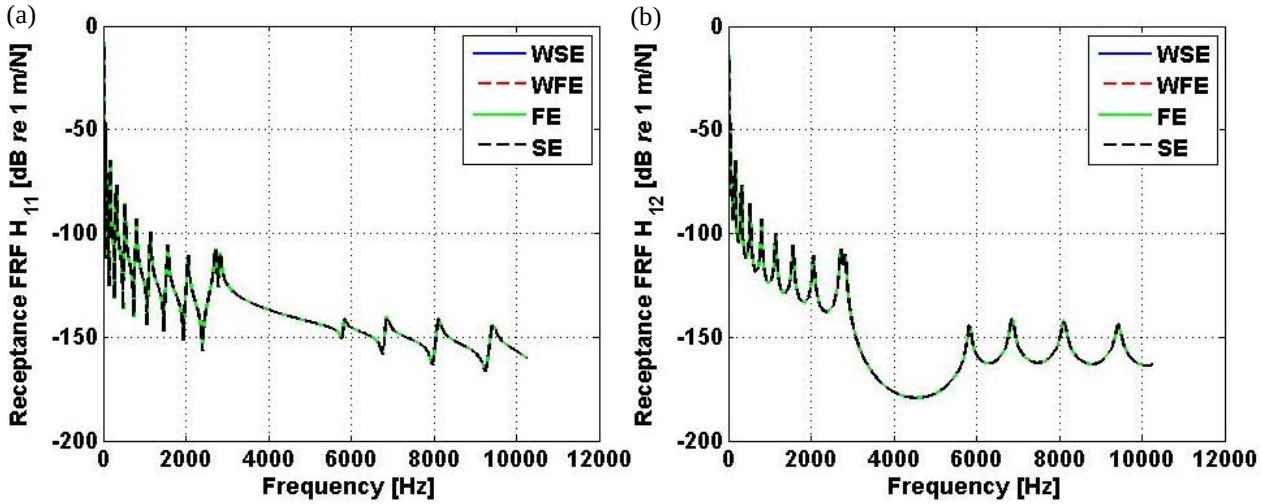

Figure 3 – Point receptance (a) and transfer receptance (b) of the PC beam calculated by the WSE, WFE, FE and SE methods showing the band gap.

From Figs. 3-4, it can be seen that the band gap is created between 2780 Hz and 5798 Hz. This band gap is known as a Bragg-type gap, because the mechanism involved is the Bragg scattering. Thus, the frequency location is governed by the Bragg condition, $a = n(\lambda/2)$, $(n = 1,2,3, \dots)$, where λ is the wavelength of waves in the host material. The Bragg condition implies that it is difficult to achieve a low frequency Bragg-type gap in PCs with small size.

In Fig. 5 (a), it is compared the transmittance for different lattice parameters calculated by WSE method until 10240 Hz. It is considered $a = 0.212,\ 0.106,\ 0.0707,\ 0.053$, which results in $N = 2, 4, 6, 8$, for the fixed beam length in Table 1. It is chosen the WSE method to compare because it is an analytical method. For the first case, $a = 0.212$, $N = 2$, it can be observed four wide Bragg-type gaps, that is to say, 122.5 Hz – 456.9 Hz, 626.3 Hz – 2884 Hz, 3174 Hz – 4439 Hz and 4439 Hz – 7961 Hz. For the other cases, $a = 0.106,\ 0.0707,\ 0.053$, $N = 4, 6, 8$, it can just be seen completely the first Bragg-type gap between 456.9 Hz – 1204 Hz , 1008 Hz – 2325 Hz and 1782 Hz – 3849, respectively. Thus, increasing the length of the unit cell, the gap will occur in low frequencies, as expected.

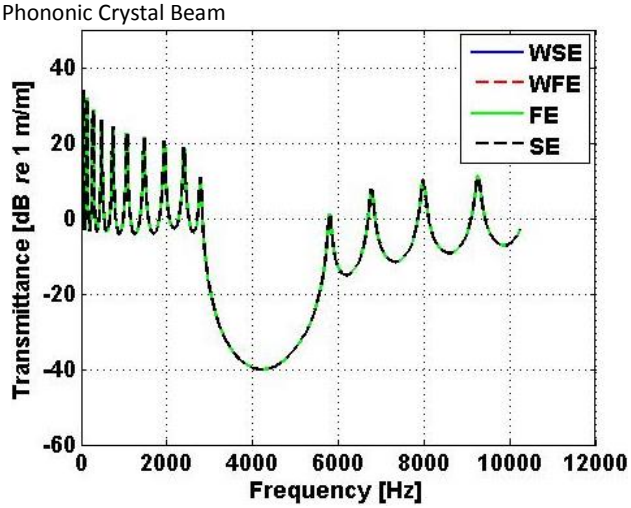

Figure 4 – Transmittance of the PC beam calculated by the WSE, WFE, FE and SE methods showing the band gap.

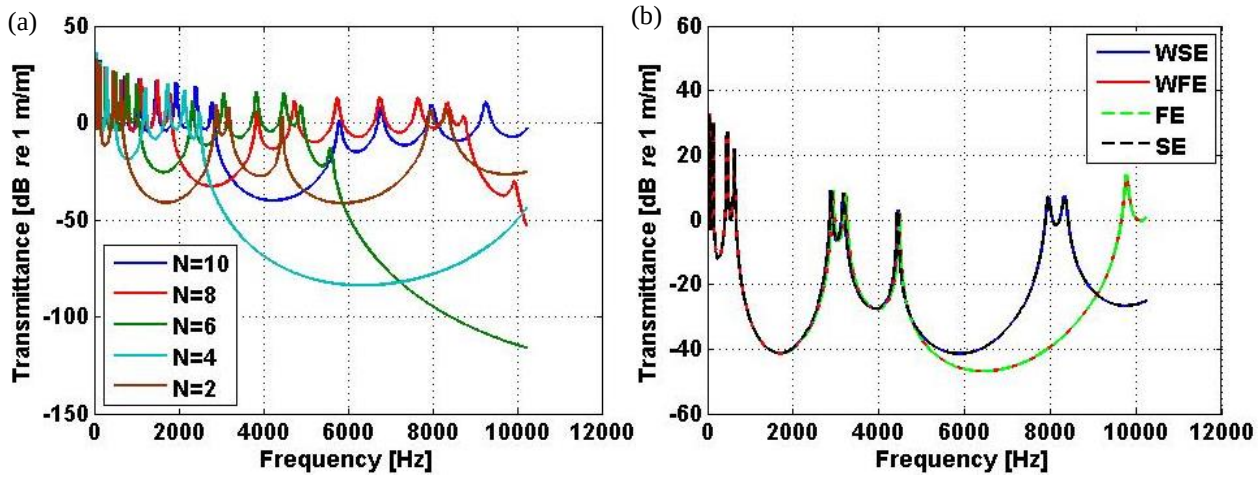

Figure 5 – Transmittance of the PC beam calculated by the WSE method for $a = 0.212,\ 0.106,\ 0.0707,\ 0.053$, $N = 2, 4, 6, 8$ (a) and the transmittance calculated by the WSE, WFE, FE and SE methods for $a = 0.212$, $N = 2$ (b).

In Fig. 5 (b) it is shown the transmittance for $a = 0.212$, $N = 2$, calculated by WSE, WFE, FE and SE methods, and it can be seen that the WFE and FE methods do not converge with WSE and SE methods in high frequencies. This happens because the discretization of the unit cell (two finite elements for each part of the unit cell, as explained before) is not enough in higher frequencies.

Figure 6 illustrates the real part of the elastic band structure, considering the data in Table 1. Figure 6 (a) shows the real part of the reduced Bloch wave vector, Ka/π, also known as wavenumber, using WSE, WFE and IPWE methods and Fig. 6 (b) shows the imaginary part of the reduced Bloch wave vector using WSE and WFE methods.

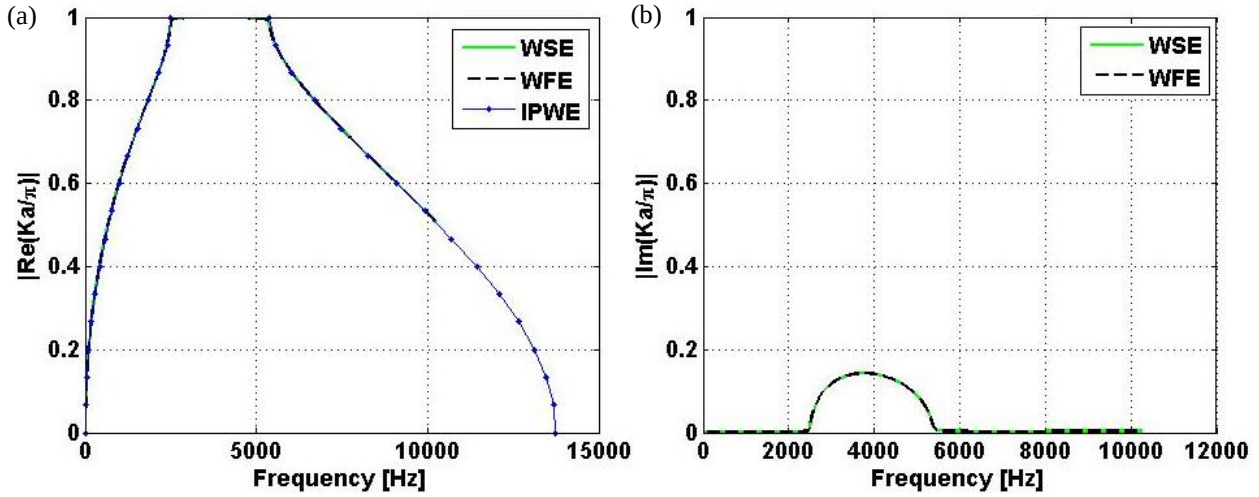

Figure 6 – Elastic band structure of the PC beam considering the data in Table 1. The real part of the reduced Bloch wave vector (a) calculated by WSE, WFE and IPWE methods and the imaginary part of reduced Bloch wave vector calculated by WSE and WFE methods.

In IPWE and CPWE calculations in this paper, it is considered 101 plane waves in the Fourier series expansion and it is only shown the irreducible Brillouin zone (IBZ) (BRILLOUIN, 1946), $[0, \pi/a]$, in Fig. 6. Figure 7 shows the comparison between the IPWE and CPWE methods inside the first Brillouin zone, *i.e.* $[-\pi/a\ , \pi/a]$.

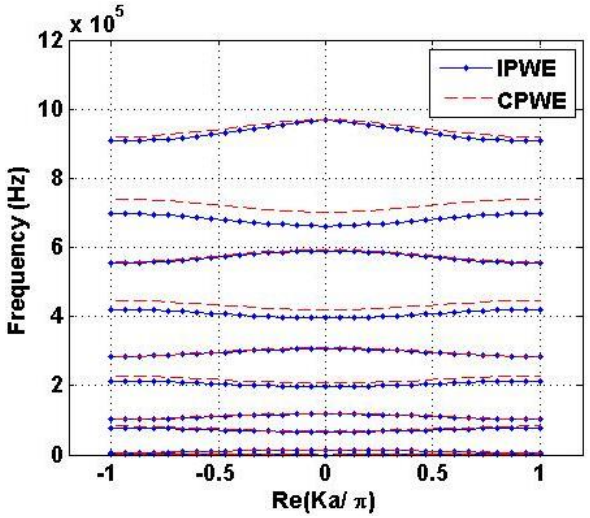

Figure 7 – The real part of the reduced Bloch wave vector calculated by IPWE and CPWE methods.

In Fig. 7, only the first 10 bands are illustrated. The convergence between IPWE and CPWE do not occur only for the high bands, even considering a high number of planes waves.

In order to demosntrated the convergence between WSE and IPWE methods for other values of a, we plot, Fig. 8 (a), the real part of the elastic band structure for $a = 0.212,\ 0.106,\ 0.0707,\ 0.053, 0.0424,\ N = 2, 4, 6, 8, 10$. Note that the curves related to each lattice parameter are not identified, but it can be seen the convergence. However, in Fig. 8 (b), this comparison is done and its behavior is the same discussed in Fig. 5 (a). The WSE method is used to calculate the imaginary part of the Bloch wave vector.

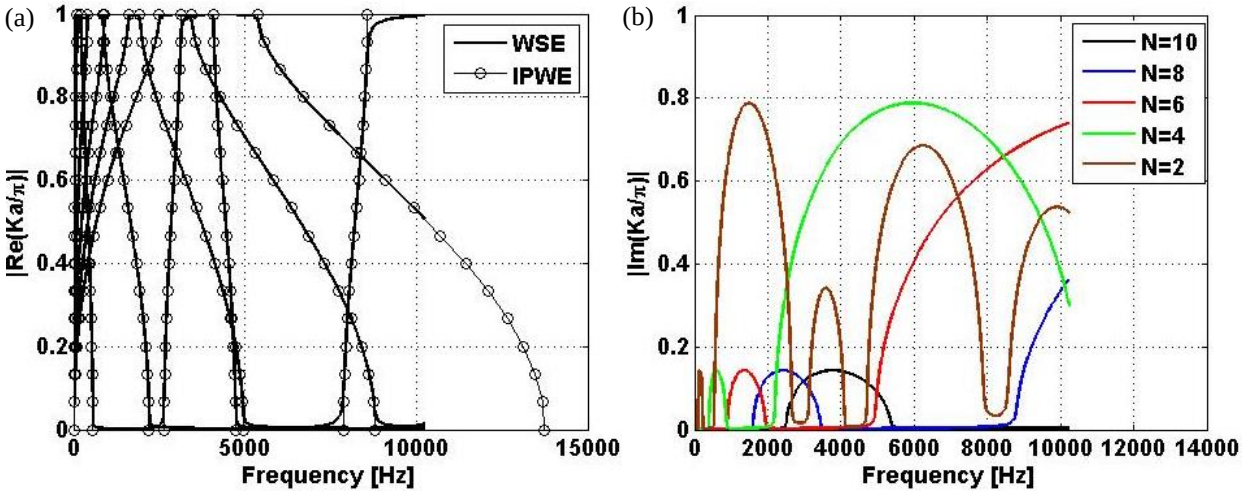

Figure 8 – Elastic band structure of the PC beam considering $a = 0.212,\ 0.106,\ 0.0707,\ 0.053, 0.0424$, $N = 2, 4, 6, 8, 10$. The real part of the reduced Bloch wave vector (a) calculated by WSE and IPWE methods and the imaginary part of reduced Bloch wave vector calculated by WSE method (b).

From Fig.8 (b), it can be seen that the attenuation performance of the Bragg-type gaps is better for $N = 2, 4$, because the existence of more gaps in low frequencies. However, the unit cell size is the limitation. The attenuation constant, defined by $\mu = -iKa$, is an important information that can be analyzed from the imaginary part of the Bloch wave vector, Fig. 8 (b), because they are related as $Re(\mu) = Im(K)a$.

Figure 9 (a-e) shows the influence of the polyethylene quantity (5% to 95%) in the unit cell for $a = 0.212,\ 0.106,\ 0.0707,\ 0.053, 0.0424,\ N = 2, 4, 6, 8, 10$, respectively. It is important to mention that until Fig. 8, it is only considered 1/3 (33,33%) of polyethylene, as described in Table 1. The polyethylene influence in the attenuation performance is complex and varies with the number of unit cells, *i.e.* with the lattice parameter, because the beam length is fixed in 0.424 m.

No attenuation is observed for $a = 0.0424$, $N = 10$ until 2500 Hz - Fig. 9 (e), $a = 0.053$, $N = 8$ until 1612 Hz - Fig. 9 (d), $a = 0.0707, N = 6$ until 874 Hz - Fig. 9 (c), $a = 0.106$, $N = 4$ until 406 Hz - Fig. 9 (b), and $a = 0.212$, $N = 2$ until 98 Hz - Fig. 9 (a), independently of the polyethylene quantity. Thus, depending on the application, choosing the polyethylene quantity correctly it is not an easy task, because it is related to the unit cell length and in which frequency the band gap start.

In Fig. 9 (b-e), there are some regions which present higher attenuation, *i.e.* between 40% - 80%, 50% - 60%, 60% - 80% and 5% - 30% of polyethyelene, for $a = 0.106,\ 0.0707,\ 0.053, 0.0424,\ N = 4, 6, 8, 10$, respectively. In Fig. 9

(a), it is difficult to identify where is the best attenuation region, because the existence of many band gaps, but below 20% of polyethyelene is the worst attenuation region.

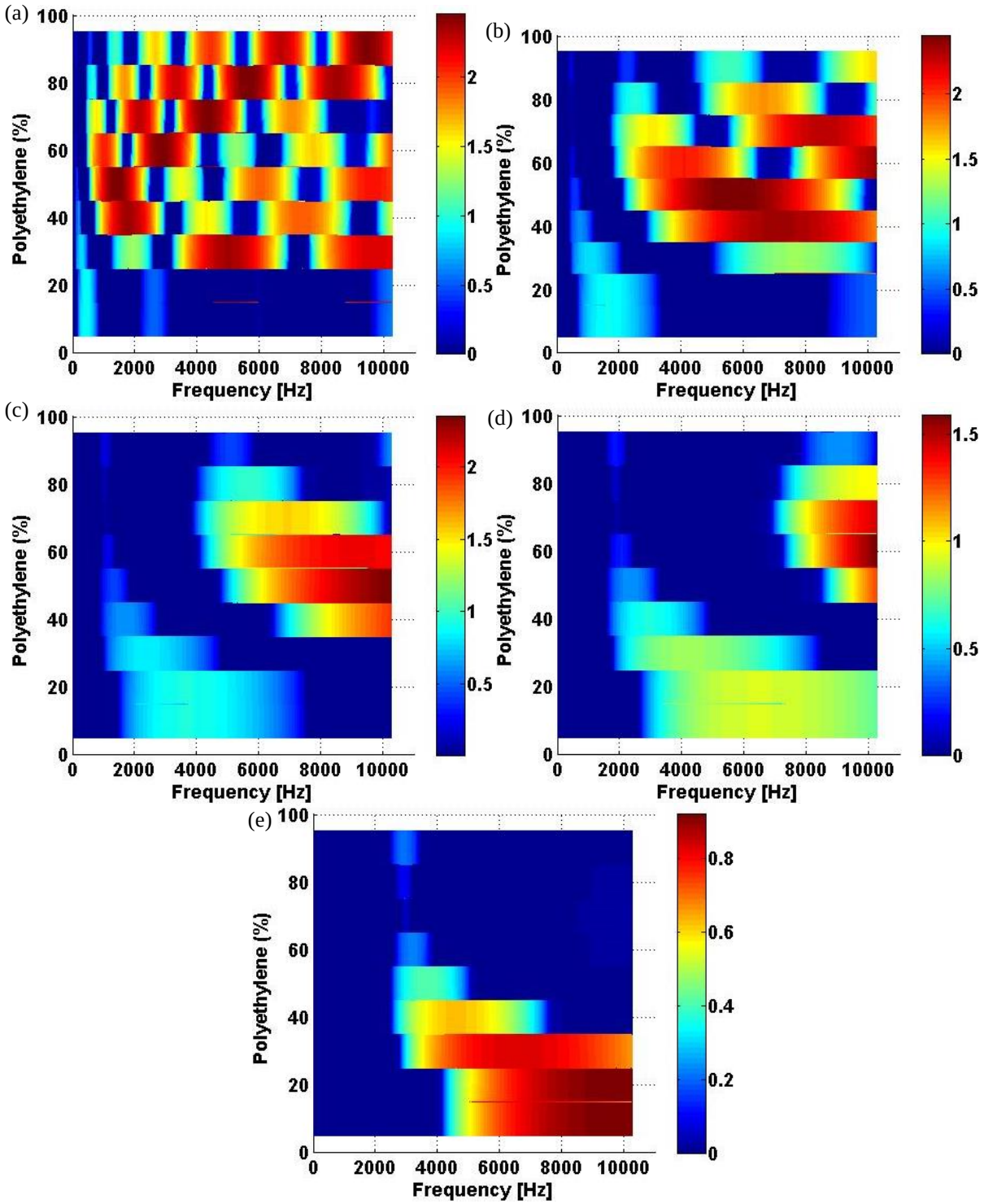

Figure 9 – Attenuation constant surface x-y view of the PC beam considering $a = 0.212,\ 0.106,\ 0.0707,\ 0.053, 0.0424$, $N = 2, 4, 6, 8, 10$, (a-e), respectively, calculated by WSE method.

Experimental validation

A real PC beam is used to perform an experimental test. The PC beam is similar to the model proposed in Fig. 1 in a free-free boundary condition, however, the $a_B = 0.041$ m and $a_A = 0.0325$ m, with $a = 2a_A + a_B = 0.106$ m. The properties are the same described in Table 1, with $N = 4$. The measurement instruments used in the experimental setup are summarized in Table 2. Figure 10 shows the experimental setup with the details of the impact hammer and accelerometers positions. By using an impact force excitation applied to the right and left ends of the PC beam, acceleration measurements are taken on the left end of the PC beam.

Table 2 – Measurement instruments.

Instrument	Manufacture and model	Sensitivity	Measure range
Impulse Hammer	PCB 86E80	22.5 mV/N	222.0 N (peak)
Accelerometer	KISTLER 8614A500M1	3.46 mV/g	(± 5%) 0-12.5 kHz
Data Acquisition	LMS SCR05	-	-

However, it is chosen to plot the displacement, that is $u = \frac{a_c}{-\omega^2}$, where u is the displacement, a_c is the acceleration measured and ω is the angular frequency. Inertance point and transfer FRFs are measured with 5 averages, with the frequency discretization of 0.625 Hz.

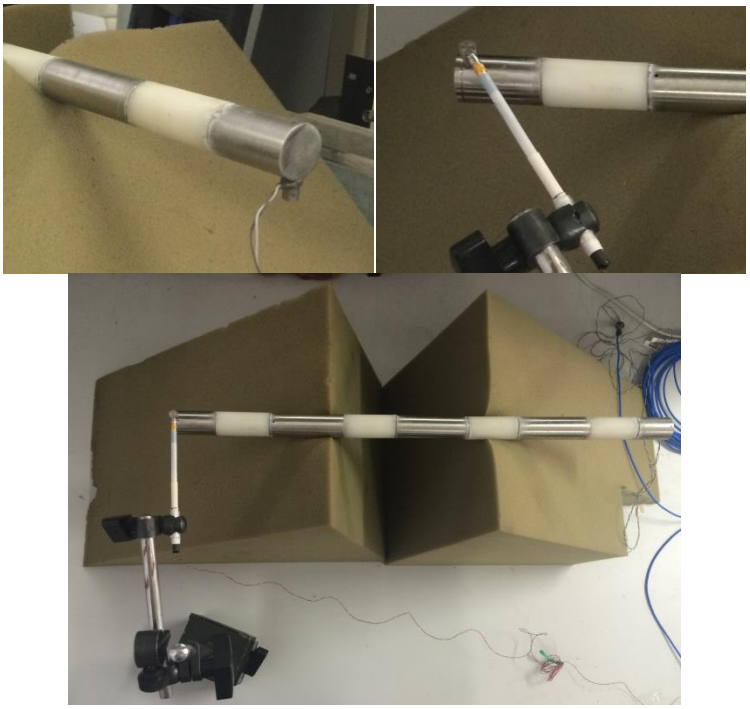

Figure 10 – Experimental setup of the PC beam.

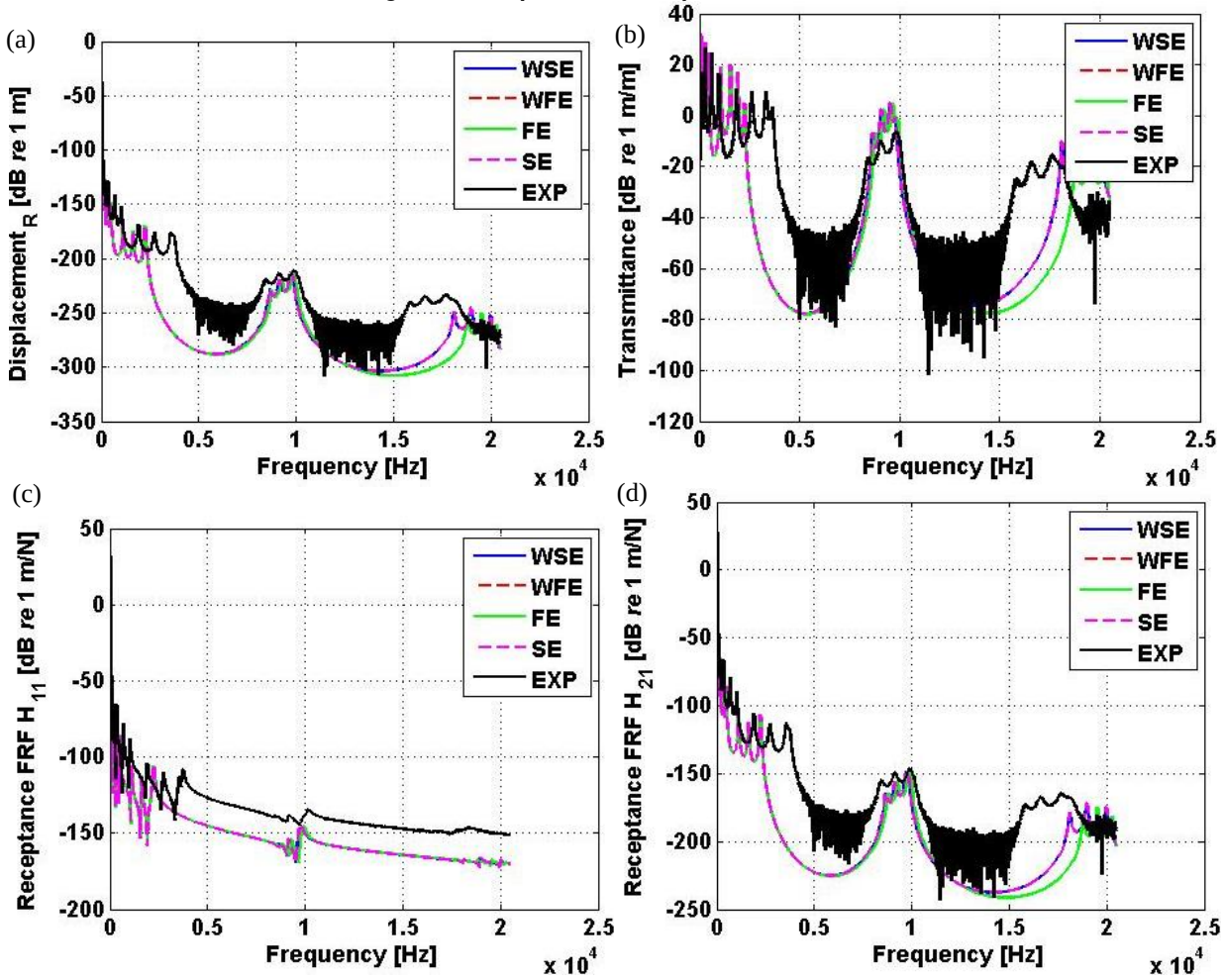

Figure 11 – PC beam displacement of the right (a) side, transmittance (b), point receptance (c) and transfer receptance (d) calculated by the WSE, WFE, FE, SE methods and measured experimentally (EXP).

Figure 11 (a-d) illustrates the displacement of the last beam node (right side), the transmittance, the FRFs H_{11} and H_{21}, respectively. The numerical results present good agreement, however, that the FE and WFE methods do not converge in higher frequencies with the analytical methods, as discussed before. Furthermore, there is some mismatch related to the experimental FRFs.

The numerical band gap widths do not converge exactly with the experimental band gaps width, as expected, because the numerical model considered may not capture all the real aspects of the PC beam, such as the material used to glue the polymer and metal, the material properties may not be exactly the same of Table 1, and others. In addition, it is used a simple EB beam theory, possibly considering higher theories, such as Timoshenko beam theory (TIMOSHENKO, 1921), the results may be improved in higher frequencies.

Figure 12 shows the elastic band structure of the real PC beam, Fig. 10, with the Bragg-type gaps. The band gaps width observed in Fig. 11 can be confirmed in Fig. 12. Furthermore, it may be observed in Fig. 12 a small gap between 405 Hz – 720 Hz with low attenuation.

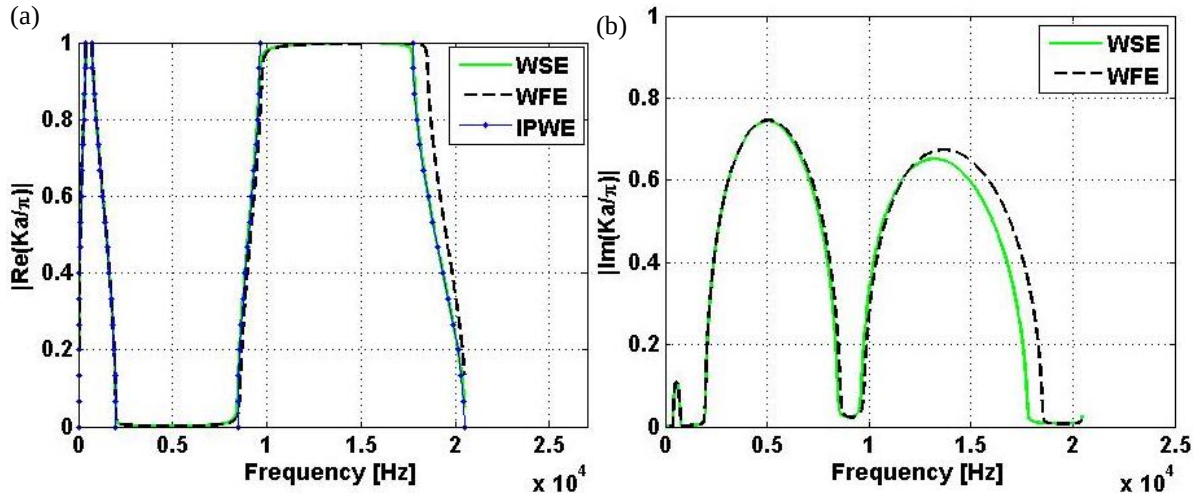

Figure 12 – Elastic band structure of the PC beam. The real part of the reduced Bloch wave vector (a) calculated by WSE, WFE and IPWE methods and the imaginary part of reduced Bloch wave vector calculated by WSE and WFE methods.

CONCLUSIONS

The forced response and the elastic band structure of a 1D PC beam are obtained. The forced response is obtained by the WFE, WSE, FE and SE methods and a good agreement is observed, instead of in high frequencies, where WFE and FE do not converge with the spectral analytical methods. The real part of the elastic band structure is calculated by the WFE, WSE and IPWE methods and it is shown a good convergence between them. The CPWE presents some disadvantages compared to the IPWE for the higher bands.

The influence of the unit cell size is also studied and for longer unit cells, that is the beam is composed by few unit cells, Bragg-type gaps are created in low frequencies. The polyethylene quantity into the unit cell is an important variable and its influence in the attenuation constant depends of the unit cell length. In some ranges of frequency, considering fixed unit cell lengths, no attenuation is observed independently of the polyethylene quantity and there are regions that present higher attenuation.

The numerical results presented illustrate a good agreement with the experimental results and they can localize the band gap position and width very close to the experimental. A small Bragg-type gap with low attenuation is observed between 405 Hz – 720 Hz. The 1D PC beam with unit cells of steel and polyethylene presents potential application for vibration management.

ACKNOWLEDGMENTS

The authors gratefully acknowledge the Brazilian research funding agency FAPEMA and IFMA for their financial support of this investigation.

REFERENCES

Anjos, V. and Arantes, A., 2015, Phononic Band Structure in Carbon Microtube Composites, RSC Advances, Vol. 5, pp. 11248-11253.

Benchabane, S., Khelif, A., Robert, L., Rauch, J.Y., Pastureaud, T. and Laude, V., 2006, Elastic Band Gaps for Surface Modes in an Ultrasonic Lithium Niobate Phononic Crystal, Proceedings SPIE, Vol. 6182, No. 618216, pp. 1-13.

Bloch, F., 1928, Über die Quantenmechanik der Electron in Kristallgittern, Zeitschrift für Physik, Vol. 52, pp. 550-600.

Brillouin, L., 1946, Wave Propagation in Periodic Structures, Dover Publications, New York, USA.

Casadei, F., Dozio, L., Ruzzene, M. and Cunefare, K.A., 2010, Periodic Shunts Arrays for the Control of Noise Radiation in an Enclosure, Journal of Sound and Vibration, Vol. 329, pp. 3632-3646.

Casadei, F., Beck, B.S., Cunefare, K.A. and Ruzzene, M., 2012, Vibration Control of Plates Through Hybrid Configurations of Periodic Piezoeletric Shunts, Journal of Intelligent Material Systems and Structures, Vol. 23, No. 10, pp. 1169-1177.

Cao, Y.J., Hou, Z.L. and Liu, Y.Y., 2004, Convergence Problem of Plane-Wave Expansion Method for Phononic Crystal, Physics Letters A, Vol. 327, pp. 247-253.

Doyle, J.F., 1997, Wave Propagation in Structures: Spectral Analysis Using Fast Discrete Fourier Transforms, 2nd ed., Springer-Verlag, New York, USA.

Floquet, G., 1883, Sur les Équations Différentielles Linéaires à Coefficients Périodiques. Annales Scientifiques de L'École Normale Supérieure, Vol 12, pp. 47-88.

Ho, K.M., Cheng, C.K., Yang, Z., Zhang, X.X. and Sheng, P., 2003, Broadband Locally Resonant Sonic Shields. Applied Physics Letters, Vol. 83, No. 26, pp. 5566-5568.

Huang, J. and Shi, Z., 2013, Attenuation Zones of Periodic Pile Barriers and its Application in Vibration Reduction for Plane Waves, Journal of Sound and Vibration, Vol. 332, pp. 4423-4439.

Jensen, J.S., 2003, Phononic Band Gaps and Vibrations in One- and Two-Dimensional Mass-Spring Structures, Journal of Sound and Vibration, Vol. 266, pp. 1053-1078.

Jian-Yu, F., Dian-Long, Y., Xiao-Yun, H. and Li, C., 2009, Coupled Flexural-Torsional Vibration Band Gap in Periodic Beam Including Warping Effect, Chinese Physics B, Vol. 18, No. 4, pp. 1-6.

Kushwaha, M.S., Halevi, P. and Martínez, G., 1994, Theory of Acoustic Band Structure of Periodic Elastic Composites, Physical Review B, Vol. 49, pp. 2313-2322.

Kushwaha, M.S. and Halevi, P., 1996, Giant Acoustic Stop Bands in Two-Dimensional Periodic Arrays of Liquid Cylinders, Applied Physics Letters, Vol. 69, No. 1, pp. 31-33.

Kushwaha, M.S., 1997, Stop-Bands for Periodic Metallic Rods: Sculptures that can Filter the Noise, Applied Physics Letters, Vol. 70, No. 24, pp. 3218-3220.

Li, L.F., 1996, Use of Fourier Series in the Analysis of Discontinuous Periodic Structures, Journal of the Optical Society of America, Vol. 13, pp. 1870-1876.

Mencik, J.-M, 2010, On the Low- and Mid-Frequency Forced Response of Elastic Structures Using Wave Finite Elements with One-Dimensional Propagation, Computers and Structures, Vol. 88, pp. 674-689.

Miranda Júnior, E.J.P. and Dos Santos, J.M.C., 2015, Flexural Wave Band Gaps in Metamaterial Elastic Beam, Proceedings of the 23rd ABCM International Congress of Mechanical Engineering, Rio de Janeiro, Brazil, pp. 1-8.

Miranda Júnior, E.J.P. and Dos Santos, J.M.C., 2016a, Phononic Band Gaps in Al_2O_3/Epoxy Composite, Submitted to Materials Science Forum, pp. 1-10.

Miranda Júnior, E.J.P. and Dos Santos, J.M.C., 2016b, Flexural Wave Band Gaps in Al_2O_3/Epoxy Composite Rectangular Plate Using Mindlin Theory, Proceedings of the 3rd Brazilian Conference on Composite Materials, Gramado, Brazil, pp. 1-8.

Miranda Júnior, E.J.P. and Dos Santos, J.M.C, 2016c, Flexural Wave Band Gaps in Elastic Metamaterial Thin Plate, Proceedings of the IX Mechanical Engineering Brazilian Congress, Fortaleza, Brazil, pp. 1-10.

Miranda Júnior, E.J.P. and Dos Santos, J.M.C, 2016d, Flexural Wave Band Gaps in Elastic Metamaterial Beam, Proceedings of the International Conference on Noise and Vibration Engineering (ISMA2016), Leuven, Belgium, pp. 2099-2113.

Ni, Z.-Q., Zhang, Z.-M., Han, L. and Zhang, Y., 2012, Study on the Convergence of Plane Wave Expansion Method in Calculation the Band Structure of One-Dimensional Typical Phononic Crystal, Optoelectronics and Advanced Materials – Rapid Communications, Vol. 6, No. 1-2, pp. 87-90.

Ni, Z.-Q., Zhang, Y., Jiang, L.-H and Han, L., 2014, Bending Vibration Band Structure of Phononic Crystal Beam by Modified Transfer Matrix Method, International Journal of Modern Physics B, Vol. 28, No. 15, pp. 1-14.

Olsson III, R.H. and El-Kady, I., 2009, Microfabricated Phononic Crystal Devices and Applications, Measurement Science and Technology, Vol. 20, No. 012002, pp. 1-13.

Pennec, Y., Vasseur, J.O., Djafari-Rouhani, B., Dobrzyński, L. and Deymier, P.A, 2010, Two-Dimensional Phononic Crystals: Examples and Applications, Surface Science Reports, Vol. 65, pp. 229-291.

Petyt, M., 2010, Introduction to Finite Element Vibration Analysis, 2nd ed., Ed. Cambridge University Press, New York, USA.

Qiu, C.Y., Liu, Z.Y., Mei, J. and Shi, J., 2005, Mode-Selecting Acoustic Filter by Using Resonant Tunneling of Two-Dimensional Double Phononic Crystals, Applied Physics Letters, Vol. 87, No. 104101, pp. 1-3.

Sigalas, M.M. and Economou, E.N., 1994, Elastic Waves in Plates with Periodically Placed Inclusions, Journal of Applied Physics, Vol. 75, pp. 2845-2850.

Timoshenko, S.P., 1921, On the Correction for Shear of the Differential Equation for Transverse Vibrations of Prismatic Bars, Philosophical Magazine, Vol. 41, No. 245, pp. 744-746.

Wang, G., Wen, J.H. and Wen, X.S, 2005, Quasi-One-Dimensional Phononic Crystals Studied Using the Improved Lumped-Mass Method: Application to Locally Resonant Beams with Flexural Wave Band Gap, Physical Review B, Vol. 71, No. 104302, pp. 1-5.

Wen, J., Wang, G., Yu, D., Zhao, H. and Liu, Y., 2005, Theoretical and Experimental Investigation of Flexural Wave Propagation in Straight Beams With Periodic Structures: Application to a Vibration Isolation Structure, Journal of Applied Physics, Vol. 97, No. 114907, pp. 1-4.

Wu, L.-Y., Wu, M.-L. and Chen, L.-W., 2009, The Narrow Pass Band Filter of Tunable 1D Phononic Crystal with a Dielectric Elastomer Layer, Smart Materials and Structures, Vol. 18, No. 015011, pp. 1-8.

Xiao, Y., Wen, J. and Wen, X, 2012, Sound Transmission Loss of Metamaterial-Based Thin Plates with Multiple Subwavelength Arrays of Attached resonators, Journal of Sound and Vibration, Vol. 331, pp. 5408-5423.

Yang, Z., Dai, H.M., Chan, N.H. and Ma, G.C, 2010, Acoustic Metamaterial Panels for Sound Attenuation in the 50-1000 Hz Regime, Applied Physics Letters, Vol. 96, No. 041906, pp. 1-3.

Yu, D., Liu, Y., Wang, G., Zhao, H. and Qiu, J., 2006a, Flexural Vibration Band Gaps in Timoshenko Beams with Locally Resonant Structures, Journal of Applied Physics, Vol. 100, No. 124901, pp. 1-5.

Yu, D., Liu, Y., Zhao, H., Wang, G. and Qiu, J., 2006b, Flexural Vibration Band Gaps in Euler-Bernoulli Beams with Locally Resonant Structures with Two Degrees of Freedom, Physical Review B, Vol. 73, No. 064301, pp. 1-5.

Yu, K., Chen, T. and Wang, X., 2013, Band Gaps in the Low-Frequency Range Based on the Two-Dimensional Phononic Crystals Plates Composed of Rubber Matrix with Periodic Steel Stubs, Physica B, Vol. 416, pp. 12-16.

Zhang, Y, Ni, Z.-Q., Han, L., Zhang, Z.-M. and Jiang, L.-H., 2012, Flexural Vibrations Band Gaps in Phononic Crystal Timoshenko Beam by Plane Wave Expansion Method, Optoelectronics and Advanced Materials – Rapid Communications, Vol. 6, No. 11-12, pp. 1049-1053.

Zhang, Y., He, J. and Jiang, L.-H, 2013, Flexural Vibration Band Gaps Characteristics in Phononic Crystal Euler Beam on Two-Parameter Foundation, Advances in Mechanical Engineering, Vol. 5, No. 935258, pp. 1-7.

RESPONSIBILITY NOTICE

The authors are the only responsible for the material included in this paper.